5-1-2020

Uranium solubility in high temperature, reduced systems

Noah van Hartesveldt

Uranium solubility in high temperature, reduced systems

By

Noah Frederick van Hartesveldt

Approved by:

Rinat I. Gabitov (Major Professor)
Brenda L. Kirkland
Artaches Migdisov
Renee M. Clary (Graduate Coordinator)
Rick Travis (Dean, College of Arts & Sciences)

A Thesis
Submitted to the Faculty of
Mississippi State University
in Partial Fulfillment of the Requirements
for the Degree of Master of Science
in Geology Concentration in Geoscience
in the Department of Geoscience

Mississippi State, Mississippi

May 2020

Name: Noah Frederick van Hartesveldt

Date of Degree: May 1, 2020

Institution: Mississippi State University

Major Field: Geology Concentration in Geoscience

Major Professor: Rinat I. Gabitov

Title of Study: Uranium solubility in high temperature, reduced systems

Pages in Study: 39

Candidate for Degree of Master of Science

The traditional paradigm declares tetravalent uranium to be immobile under reducing conditions – an assumption widely employed for nuclear waste management strategies. In contrast, experiments presented here demonstrate this assumption, although valid for low temperatures, can be erroneous for high temperature natural systems. This project focuses on the ability of sulfate-bearing solutions to transport uranium at reduced conditions and elevated temperatures, identifies the new species $U(OH)_2SO_4$, derives thermodynamic constants necessary for modeling, and expands the quantifiable range of U^{4+} mobility to more neutral pH conditions. The data obtained enable more accurate assessment of uranium mobility by updating the existing uranium thermodynamic databases and is applicable to uranium fluid transport in ore-forming systems and nuclear waste repositories.

ACKNOWLEDGEMENTS

To the EES-14 team at Los Alamos National Laboratory and the Department of Geosciences at Mississippi State University for their support. Sincere appreciation to Rinat Gabitov and Artas Migdisov for their advising and continued reviews of the manuscripts from which this thesis evolved.

TABLE OF CONTENTS

LIST OF TABLES

LIST OF FIGURES

CHAPTER I

INTRODUCTION

1.1 Scope and Purpose

The scope of this research covers high temperature, aqueous uranium geochemistry. The purpose of the experiments presented is to fill gaps in the fundamental understanding of uranium behavior at elevated temperatures in aqueous solutions. In turn, this will ultimately enable the ability to model uranium behavior at hydrothermal conditions and improve actinide geochemistry modelling, as a whole. The study involved laboratory experiments performed at elevated temperature and pressure. Experimental data were used to derive thermodynamic constants, which then can be used in the following models of natural and man-made systems: nuclear waste disposal, hydrothermal ore formation, reactor accident contamination spread, and more. These models will provide enhanced safety protocols with improved predictive capabilities and will facilitate more efficient natural resource exploration.

1.2 Background

1.2.1 Uranium in Nature

Uranium in nature most commonly forms complexes in one of two valence states: U^{4+} and U^{6+} (Bastrakov, Jaireth, & Mernagh, 2010). At room temperature, solid uranyl (U^{6+}) compounds are soluble, and form stable species in aqueous solutions (Guillaumont et al., 2003). Contrary to the oxidized species, solid uranous (U^{4+}) compounds have very low solubility in aqueous solutions at standard temperature (referred as low temperature further in the text) and

pressure (i.e. 25°C and 1 bar), (Guillaumont et al., 2003). As a result, low temperature, aqueous system species distributions are characterized predominantly by U(VI) species. These U(VI) species are expected to control uranium mobility – a paradigm of most existing geochemical models (Cuney, 2009; Haynes, Cross, Bills, & Reed, 1995; Komninou & Sverjensky, 1995; Richard et al., 2011). From these observations, models regularly use a change in oxidation state to explain uranium mobilization and deposition in ore deposits, to justify uranium waste disposal site choices, and to quantify the spread of uranium contamination in cases of nuclear reactor disasters. Although these existing models (based on data obtained at low temperatures) are being used to describe the natural, hydrothermal systems (Ahonen, Ervanne, Jaakkola, & Blomqvist, 1994; Rich, Holland, & Peterson, 1977; Sunder, Cramer, & Miller, 1996), our data show that oxidation state cannot solely control uranium behavior at high temperatures.

1.2.2 High Temperature Speciation

The data for high temperature aqueous speciation of uranium is significantly lacking in the literature (Guillaumont et al., 2003). Existing reliable high temperature experimental studies are limited to U^{4+}-OH^- complexes (Parks & Pohl, 1988; Tremaine, Chen, Wallace, & Boivin, 1981), while uranous complexation with other ligands (chloride, sulfate, carbonate, etc.) has historically been considered insignificant (Grenthe et al., 1992; Guillaumont et al., 2003). However, recent work has shown orders of magnitude higher stability of aqueous U(IV) chloride species. These findings question the efficacy of existing elevated temperature models, but primarily at low pH conditions – not as likely to be observed in repository systems (Timofeev et al., 2018). Sulfate, like chloride, is highly abundant in natural waters, but SO_4^{2-} is also available for complexation in more neutral-range pH systems. According to hard-soft acid-base theory, sulfate, a hard base, should readily complex with uranium, a hard acid. The initial high

temperature chloride experiments directly challenge the existing paradigm that reducing conditions ensure uranium immobilization. Therefore, the focus of this work involves uranium complexation with SO_4^{2-} to challenge the paradigm at a larger range of conditions.

1.2.3 Sulfate System

Sulfate is abundant in the seawater that played an active role in the Fukushima disaster (Millero, Feistel, Wright, & McDougall, 2008), is expected to be present in solutions that may interact with nuclear waste disposal sites (Caporuscio, Palaich, Cheshire, & Jové Colón, 2017; M. C. Cheshire, Caporuscio, Jové Colón, & Norskog, 2018; Michael C. Cheshire, Caporuscio, Rearick, Jové-Colón, & McCarney, 2014), and is also a typical feature of many uranium-ore forming fluids (Gammons, Wood, Jonas, & Madison, 2003; Kister, Vieillard, Cuney, Quirt, & Laverret, 2005). Previous experimental studies performed at ambient and near-ambient temperatures demonstrate high affinity of U(IV) to the sulfate ligand and high stability of USO_4^{2+} and $U(SO_4)_2^0$ aqueous species, relative to other U(IV) complexes (Hennig et al., 2007; Perez, Gil, & Gil, 1980). Moreover, while there is limited data for U(VI) sulfate species $(U)SO_4^0$ and $UO_2\ (SO_4)_2^{2n}$ at ambient conditions, high temperature experimental data is still lacking (Guillaumont et al., 2003). Therefore, the principle goal of these experiments is to investigate speciation of U(IV) in sulfate bearing solutions at elevated temperatures, then derive quantitative thermodynamic data characterizing the stability of the observed uranous sulfate species.

CHAPTER II

EXPERIMENTAL METHODS

2.1 Experimental Technique

To determine uranium speciation with sulfate, all experiments presented employ the autoclave solubility method. The experiments involve determining the solubility of UO_2 (Uraninite, reference phase) at various temperatures, concentrations of sulfate, pH, and redox conditions. Redox control was performed using the solid-state redox buffers approach (see 2.2.2). The advantage of the autoclave technique is the ability to work with very low uranium concentrations, which are expected in U(IV) systems.

Experiments were performed in titanium, light-weight autoclaves that provide a chemically inert reaction vessel, and a Teflon liner was also used to provide an additional measure of ensuring chemical inertness for experiments at 250°C. The process of assembling experiments is outlined. First, experimental solutions were prepared from de-ionized, nano-pure water and Na_2SO_4 (Fisher Scientific, A.C.S.), with sulfate concentrations ranging from 0.05 to 0.55 mol/L then loaded into the autoclaves, and solutions' pH_{25^oC} were adjusted to approximately 2 using HCl (Fisher Scientific, Optima grade). Table 1 in Appendix A provides detailed tabulations for each experimental point.

After this, short, test tube-like holders (one end open, fused quartz tubes) containing UO_2 (99.8% International Bio-Analytical Industries, Inc.), long holders containing solid-state redox buffers (Ni/NiO or Co/CoO; Fisher Scientific, 99.95%) were added, and the autoclaves were

flushed with Argon gas (Matheson Tri Gas, Ultrapure). Flushing removes excess atmosphere oxygen from the system. By doing this fO_2 re-equilibration was accelerated, and unnecessary consumption of the buffers by atmospheric oxygen was prevented. Finally, a Grafoil® O-ring seals the autoclaves as the caps were tightened, then placed into furnace preheated to desired temperature (see 2.1.2). A schematic of the experimental setup is illustrated in Figure 2.1.

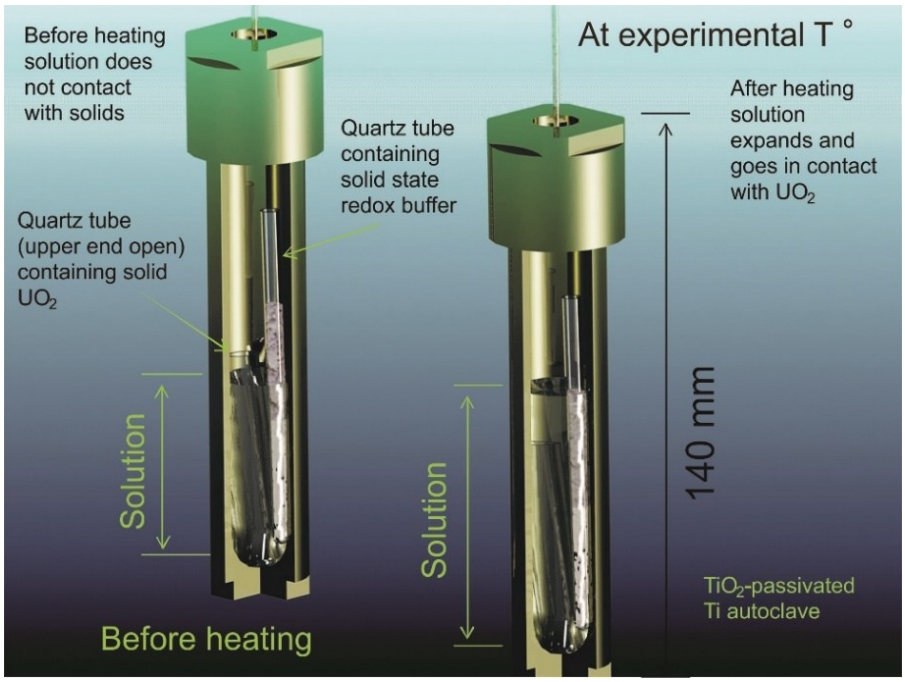

Figure 2.1 Experimental setup

A sketch of the experimental setup. Titanium autoclaves house one short and one long holder containing UO_2 and a solid-state redox buffer, respectively. Solution is added, and thermal expansion immerses the short holder at the maximum experimental temperature.

2.1.2 Ensuring Reducing Conditions

The solid-state redox buffers used in all experiments are a mixture of two compounds containing the same element in different valence states (typically metal/oxide or oxide/oxide).

When both compounds are present in the system, the fugacity of oxygen (f_{O2}) can be expressed through redox reaction, and is thus strictly defined at each given temperature. For example,

$$Ni^{metal} + 0.5O_2^{gas} = NiO^{solid} \quad (2.1)$$

And

$$\log fO_2 = -2log(K_T) \quad (2.2)$$

where K_T is the thermodynamic constant of the reaction at a given temperature.

The majority of experiments were performed using Ni/NiO solid-state redox buffers. As a check for the assumption that data collected using the Ni/NiO buffers kept dissolved uranium in the U(IV) redox state, a few control experiments were run with Co/CoO solid-state redox buffer. If the dissolution of UO_2 is mostly controlled by U(IV) aqueous species, then the system will be redox independent, and experiments run using the same solution chemistry but different redox buffers (Ni/NiO and Co/CoO set ~3 orders of magnitude different fO_2) should be identical, e.g.:

$$UO_2^{solid} + 4H^+ = U^{4+} + 2H_2O \quad (2.3)$$

If the predominant species observed is a uranyl compound, then the solubility of UO_2 is a redox-dependent reaction, according to the reaction:

$$UO_2^{solid} + 2H^+ + 0.5O_2^{gas} = UO_2^{2+} + 2H_2O \quad (2.4)$$

Therefore, agreement of solubility measurements using both Ni/NiO and Co/CoO solid-state buffers is qualifying criteria for predominance of U(IV) species.

2.1.3 Sulfate Activity Model and its Selection

All experimental solutions were prepared using NaCl (Fisher Scientific, A.C.S.) as a background electrolyte at the concentration of 1 mol/kg H_2O, since the most reliable and experimentally best-tuned activity model valid for high temperature ionic solutions was developed for NaCl-dominated solutions (recommended for ionic strengths up to I = 6 and temperatures up to T = 600°C) (Helgeson, Kirkham, & Flowers, 1981; Oelkers & Helgeson, 1990, 1991).

The chemical activity of a dissolved component is always different from its concentration. Chemical activity is a measure of the active concentration of a substance at a given state relative to its chemical potential at its standard state, and thermodynamics describes these deviations from the ideal behavior through activities and activity coefficients (Anderson & Crerar, 1993). Likewise, thermodynamic constants, the main aim of this study, are expressed through activities, and therefore, require a reliable and experimentally proven activity model. A variety of activity models are available, but due to the empirical basis of most, they are not applicable to the elevated temperature systems used in these experiments. Electrolyte solutions introduce further complications, as compounds dissociate, and ionic strength becomes an important variable, so it is necessary to choose a model experimentally proven for both elevated temperatures and high ionic strength.

All calculations reported here employ the extended Debye-Huckel model, modified by Helgeson et al. (1981), Oelkers and Helgeson (1990), and Oelkers and Helgeson (1991) for NaCl-dominated solutions:

$$\log \gamma_i = - \frac{A \cdot [Z_i]^2 \cdot \sqrt{I}}{1 + B \cdot \mathring{a} \cdot \sqrt{I}} + \Gamma + b_\gamma I \quad (2.5)$$

where A and B are the Debye–Huckel parameters, Z_i, Γ and $\mathring{a}$ are the individual molal activity coefficient, the charge, a molarity to molality conversion factor and the distance of closest approach of an ion i, respectively. The effective ionic strength calculated using the molal scale is I and b_γ is the extended-term parameter for NaCl dominated solutions.

2.1.4 Stage Heating and System Equilibration

Autoclaves were heated in a ThermoFisher Scientific Thermolyne Largest Tabletop Muffle Furnace (±0.5 C). Thermal expansion of the solution was used to ensure the measured solubility corresponds only to the maximum experimental temperature – not to intermediate, ramp stage temperatures. The volume of experimental solutions placed in the autoclaves was calculated to ensure the solution was not in contact with the UO_2 reference phase at room temperature. Heating was initialized at a ramp temperature less than the experimental temperature to provide time for the slower kinetics of the solid-state buffers (see below) to equilibrate the system to reducing fO_2 conditions. As a result of the thermal expansion calculations, the expanded solution did not come above the short UO_2 holder at this stage.

Once fully equilibrated, the furnace temperature was increased to the maximum, experimental temperature. After, solution expanded again and flushed the short UO_2 holder, while the tall holder with the redox buffer remained out of contact with the solutions. When the experiments were removed from the oven and rapidly quenched, the solution contracted and lost contact again as the temperature returned to ambient. This technique ensured that the solubility measured during the experiments closely reflected the solubility at experimental temperature and

was not affected by the processes that may've occurred during the quenching or heating of the autoclave.

Finally, a time series of experiments at identical chemical conditions (constant SO_4^{2-}, pH) was performed prior to experiments to determine the time required to attain equilibrium (steady state). This established the one-day minimum time required for the systems to reach equilibrium and saturation with respects to uranium. This is presented graphically in Experimental Results section.

2.1.5 Post-experiment Processing

After the solutions were heated at experimental temperature and reached equilibrium, the autoclaves were removed from the oven and air quenched until the solution reached room temperature. Holders containing UO_2 and fO_2 buffers were removed, and aliquots of post-experimental solutions were taken for sulfate and pH controls. The sulfate concentration was analyzed using High Pressure Liquid Chromatography (HPLC), and pH was measured potentiometrically. After pH measurement, concentrated HNO_3 (Fisher Scientific, TM grade) was added to the autoclave to dissolve any uranium which may have precipitated from solutions on the inside walls of the autoclave during cooling. Autoclaves were left to soak overnight before an aliquot of the acidified experimental solution was removed to measure total dissolved uranium. To ensure all deposited uranium was dissolved, a second acid rinse was left to soak overnight after the experimental solution was removed. Results showed residual uranium concentrations in the second rinse solution were negligible.

Inductively Coupled Plasma Mass Spectrometry (ICP-MS) was used to measure uranium concentration, and was independently confirmed using Kinetic Phosphorimetry Analysis (KPA). Lastly, to ensure that the measured solubility corresponded only to the dissolution of UO_2 (no

changes to the reference solid phase throughout the course of the experiments), random holders were selected post experiment, and solids were analyzed by X-ray diffraction. Examples of the XRD spectra taken from post-experimental solids are illustrated in Figure 3.1.

CHAPTER III

RESULTS AND DISCUSSION

3.1 Experimental Results

A complete, tabulated summary is presented in Table 3.1. Each experiment is identified by maximum experimental temperature (T ºC), solid-state redox buffer (buffer), ligand concentration (measured, HPLC confirmed), pH (25ºC and max T), and uranium concentration (ppm and log m).

Table 3.1 Experimental solution descriptions

T ºC	Buffer	Na_2SO_4 (mol/Kg)	HPLC Na_2SO_4 (mol/Kg)	pH (25ºC)	pH (T)	Uranium (ppm)	Uranium (log m)
250	Ni/NiO	0.001	0.001	3.300	3.803	0.065	-6.483
250	Ni/NiO	0.005	0.005	2.880	3.821	0.287	-5.840
250	Ni/NiO	0.008	0.008	2.740	3.855	0.409	-5.685
250	Ni/NiO	0.01	0.010	2.650	3.841	0.655	-5.481
250	Co/CoO	0.025	0.027	2.350	3.932	0.958	-5.316
250	Co/CoO	0.05	0.054	2.150	4.026	1.160	-5.233
250	Ni/NiO	0.08	0.083	2.090	4.187	1.164	-5.231
250	Ni/NiO	0.1	0.103	1.990	4.168	1.376	-5.159
250	Ni/NiO	0.025	0.025	2.960	4.623	0.061	-6.512
250	Ni/NiO	0.025	0.026	2.900	4.555	0.069	-6.459
250	Ni/NiO	0.025	0.026	2.630	4.264	0.312	-5.803
250	Co/CoO	0.025	0.026	2.570	4.199	0.379	-5.718
250	Co/CoO	0.025	0.025	2.560	4.186	0.368	-5.732
250	Ni/NiO	0.025	0.026	2.510	4.130	0.348	-5.756
250	Ni/NiO	0.025	0.027	2.310	3.876	1.013	-5.292
250	Ni/NiO	0.025	0.026	2.130	3.625	3.764	-4.722
300	Ni/NiO	0.05	0.046	2.353	4.555	1.171	-5.309
300	Ni/NiO	0.05	0.042	2.165	4.754	0.283	-5.925
300	Ni/NiO	0.25	0.239	2.091	4.689	2.336	-5.009
300	Ni/NiO	0.25	0.260	1.997	4.751	0.923	-5.412
300	Co/CoO	0.25	0.248	2.314	4.929	0.633	-5.576
300	Ni/NiO	0.35	0.354	2.091	4.851	1.717	-5.142
300	Ni/NiO	0.35	0.313	2.227	5.100	0.719	-5.520
300	Ni/NiO	0.45	0.451	2.095	4.894	1.306	-5.261
300	Ni/NiO	0.55	0.546	2.050	4.880	1.451	-5.215
350	Ni/NiO	0.05	0.053	2.436	5.261	0.067	-6.550
350	Co/CoO	0.05	0.034	2.036	4.723	0.293	-5.910
350	Ni/NiO	0.05	0.034	1.897	4.480	1.595	-5.174
350	Ni/NiO	0.15	0.144	2.110	5.189	0.602	-5.597
350	Co/CoO	0.15	0.135	2.133	5.216	0.665	-5.555
350	Ni/NiO	0.15	n.a.	1.709	4.674	1.420	-5.225
350	Ni/NiO	0.25	0.222	1.836	4.968	2.905	-4.914
350	Ni/NiO	0.25	0.232	2.050	5.211	0.381	-5.797
350	Co/CoO	0.25	0.264	2.193	5.371	0.253	-5.975
350	Ni/NiO	0.35	0.351	2.051	5.254	0.615	-5.588
350	Co/CoO	0.35	0.336	2.288	5.504	0.294	-5.908

Composition of experimental solutions, solid-state buffer used, pH_{25^oC} measured after quenching, and pH_T extrapolated to maximum experimental temperature.

3.1.2 XRD Spectra

The reference phase ($UO_2^{cryst.}$) was analyzed post-experiment to confirm no alteration or oxidation to U(VI) over the course of the experiment. The XRD spectra taken from post-experimental solids are illustrated in figure 3.1. Results do not suggest any alteration of the reference phase as only UO_2^{cryst} was detected. The minor offset peaks are likely due to oxidation during storage time when reducing conditions were not maintained, such as during transport and while in storage.

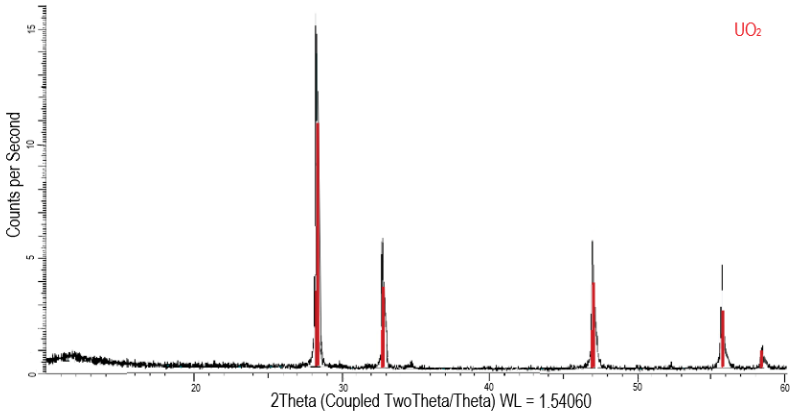

Figure 3.1 Sulfate Series XRD Spectra

Spectra results showing close match between the predicted diffraction peaks (red) for UO_2 and those observed in the experiment.

3.1.3 Kinetic Series

A set of 7 experiments with identical sulfate concentration (Na_2SO_4 = 0.4 mol/kg) and pH ranging from 2.1 to 2.3, was performed at 250ºC for durations of 1 to 7 days to determine the time needed to reach equilibrium (figure 3.2). After four days at 250ºC, uranium concentrations reached a plateau, and remained here for the duration of the experiments. Equilibrium is

expected to be reached sooner at elevated temperatures. Therefore, the consistent uranium concentrations beyond four days suggest the concentration measured for any experiment exceeding four days will also correspond to isothermal solubility. As an additional precaution to ensure system equilibrium is attained, all experiments reported in this study were run for a minimum of six days.

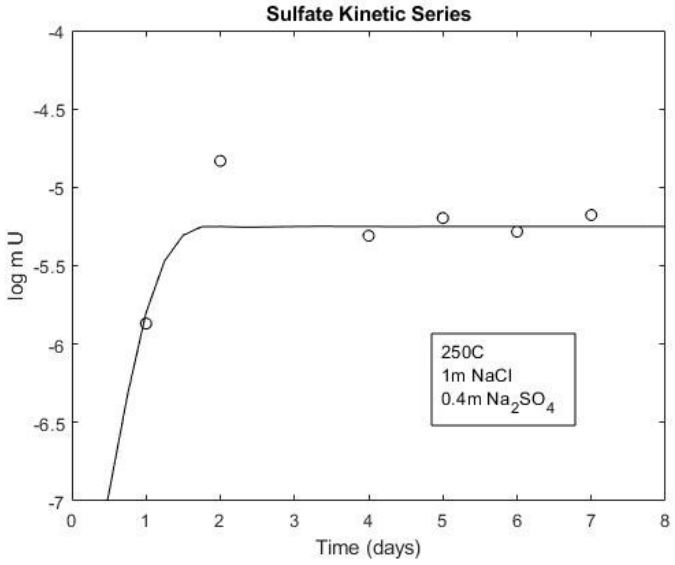

Figure 3.2 Sulfate Kinetic Series

Experiments were performed at 250°C. Equilibrium was attained after approximately three days.

3.1.4 pH Effects

The initial model used for preliminary pH calculations and sulfate species activities was calculated using the Hch package to minimize the Gibbs free energy of the chemical system. The model includes H_2O, H^+, OH^-, O_2, H_2, Na^+, $NaOH^0$, $NaSO_4^-$, $NaCl^o$, SO_4^{2-}, HSO_4^-, Cl^-, and HCl^o, and all thermodynamic data for calculations presented are from Johnson et al. (1992),

Sverjensky et al. (1997), and Tagirov et al (1997). Although both the initial pH values of experimental solutions and those measured after the experiments ($pH_{25°C}$) are all appreciably acidic (1.7-3.3), pH values *calculated* for experimental temperatures (pH_T), especially at 300°C and 350°C, are shifted to near-neutral range (Table 3.1). This effect is due to two related factors. First, sulfuric acid strength significantly decreases with temperature (e.g. the pK of the dissociation reaction, $HSO_4^- = H^+ + SO_4^{2-}$, changes from 1.97 (25 °C) to 7.40 (350°C) at saturated water pressure; figure 3.3). Second, the pH_T of an experimental solution is largely controlled by weak-acid/strong-base interactions: a result of using Na_2SO_4 to set sulfate concentrations.

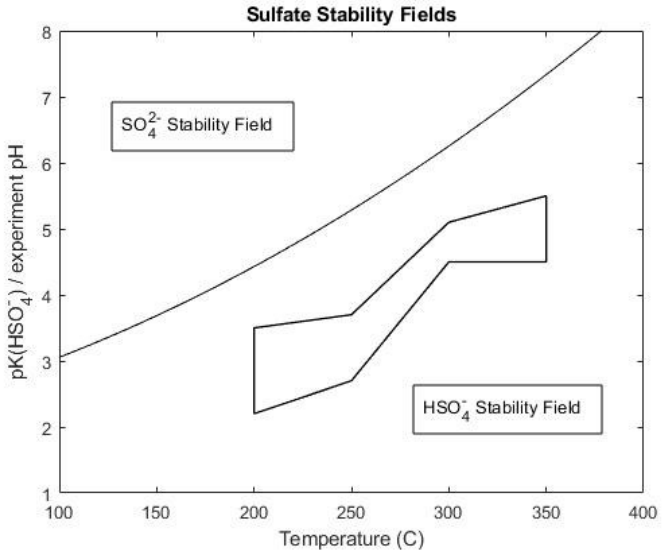

Figure 3.3 Sulfate Stability Fields

The values of the dissociation constant of sulfuric acid ionized in water (pK $HSO_4^- = H^+ + SO_4^{2-}$) and the range of pH_T investigated in the experiments as a function of temperature (polygon).

3.1.5 Thermochemical Sulfate Reduction

Concentrations of total sulfate added to the solutions pre-experiment and those measured post-experiment using high pressure liquid chromatography (HPLC) were presented in Table 3.1. These results are indistinguishable within experimental error. The redox conditions present in the experiments correspond to the predominance fields of H_2S and HS^- species (fig. 3.4a). If equilibrium is established, then SO_4^- would represent a small proportion of dissolved sulfur at the low fugacity, experimental conditions. However, thermochemical sulfate reduction (TSR) process is known to be characterized by slow kinetics, and the process often requires additional species such as polysulfanes or polythionates to initiate (Ellis et al., 2016; Goldstein & Aizenshtat, 1994; Li, Cai, Jia, Xu, & Zhang, 2017; Thom & Anderson, 2008). Figure 3.4b demonstrates this process did not initiate (at a detectable level), since initial and final concentrations of sulfate are equivalent. For derivations presented in this study, the 'frozen' sulfur redox equilibria are assumed, and concentrations of sulfate control uranium speciation (fig. 3.3).

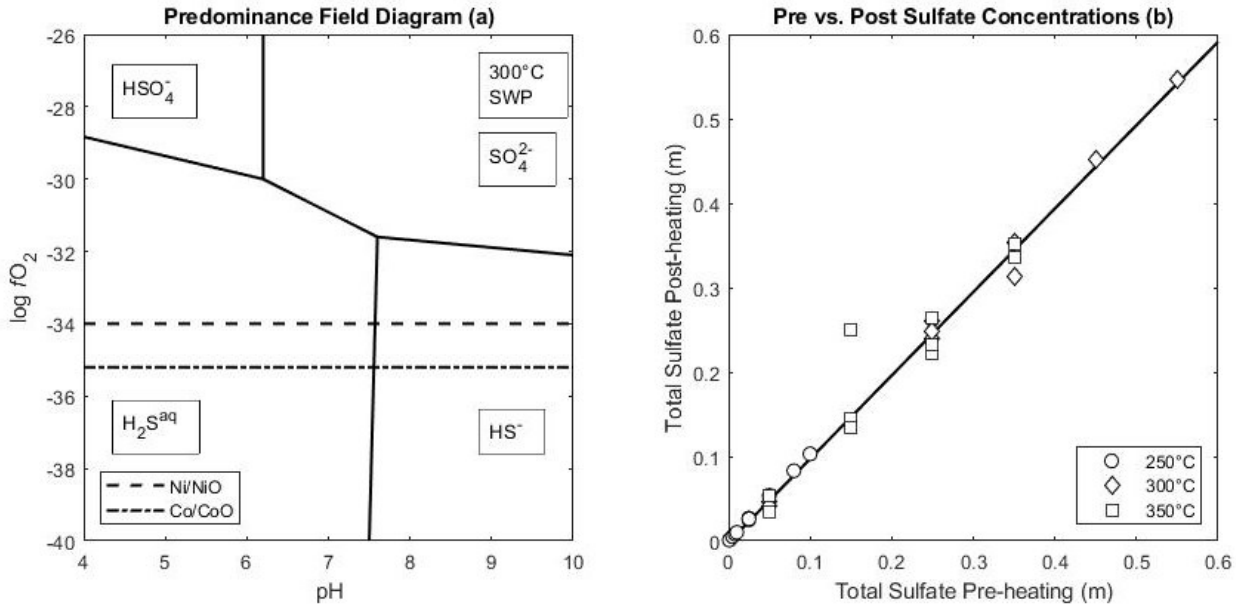

Figure 3.4 Predominance Field Diagrams and Thermochemical Sulfate Reduction

(A): Predominance field diagram for aqueous sulfur species at 300°C. Dashed lines indicate experimental conditions with solid-state redox buffers of Ni/NiO or Co/CoO. (B) Pre-experimental sulfate concentrations plotted against post-experimental measurements, demonstrating the lack of sulfur reduction suggested in the predominance field diagrams.

In the high temperature experiments performed without Teflon lining (300-350°C), the $pH_{25°C}$ increases more significantly. This effect can be explained by minor interactions of acid in the solution with the autoclave wall, subsequently neutralizing the solution. While this shift does not exceed 0.1-0.5 $pH_{25°C}$ units, it does lead to significant pH_T variance, which adds additional variability to the UO_2 solubility controls. Therefore, UO_2 solubility data reduction must assume dependence on both pH_T and sulfate concentration.

3.1.6 $U(OH)_2SO_4^\circ$ Stoichiometry

By varying sulfate concentration in solution, we are able to demonstrate uranium concentration dependency. The logarithm of measured uranium concentration (mol/kg) is plotted

as a function of the logarithm HSO_4^- of activity calculated for each data point. This yields a stoichiometric ratio ($U:HSO_4^-$). The data was fit with a linear regression, and the slopes (y = mx + b, where m = slope) of the data for the three isotherm temperatures (250, 300, and 350°C) range from 0.958 to 1.760 (figure 3.5). The raw data dependencies do not reflect the stoichiometric ratios of the predominant aqueous species; rather, they are a dependency of both hydrosulfate and proton activity (HSO_4^- and pH).

The pH change from 25ºC to T_{max}ºC increases at each isotherm, so it can be assumed that isotherm curve at 250°C represents a closer approximation to the true stoichiometric ratio of the predominant species ($U:HSO_4^- = 1:1$). With this initial hypothesis, the data was normalized assuming a 1:1 stoichiometric ratio and plotted as a function of pH_T to evaluate the effect of pH on total UO_2 solubility (figure 3.6). Normalization standardizes experimental values by fixing HSO_4^- activity. The difference between the fixed and experimental value is multiplied by the 1:1 stoichiometric ratio. This value is divided by the logarithm of uranium concentration, so proper stoichiometric slopes can be observed when logarithms of uranium concentrations are plotted against pH. All isothermal curves show an inverse linear dependency (m = -1) of uranium concentration on pH.

Using the pH dependency to adjust for pH change in the experimental solutions, we validated the original hypothesis that the predominate uranium species are characterized by the stoichiometric ratio $U:HSO_4^- = 1:1$. After normalizing the data for pH dependency, uranium concentrations now show a close linear dependency (m = 1) on HSO_4^- activity (figure 3.7).

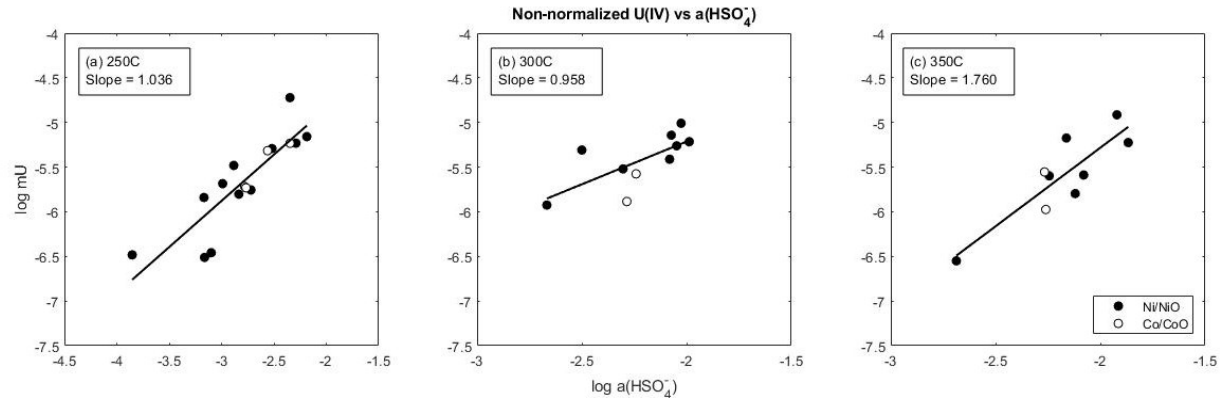

Figure 3.5 Non-normalized function of uranium concentrations vs HSO_4^- activity

Logarithms of uranium molality plotted as a function of increasing HSO_4^- activity at three isotherms: (a) 250°C, (b) 300°C, and (c) 350°C.

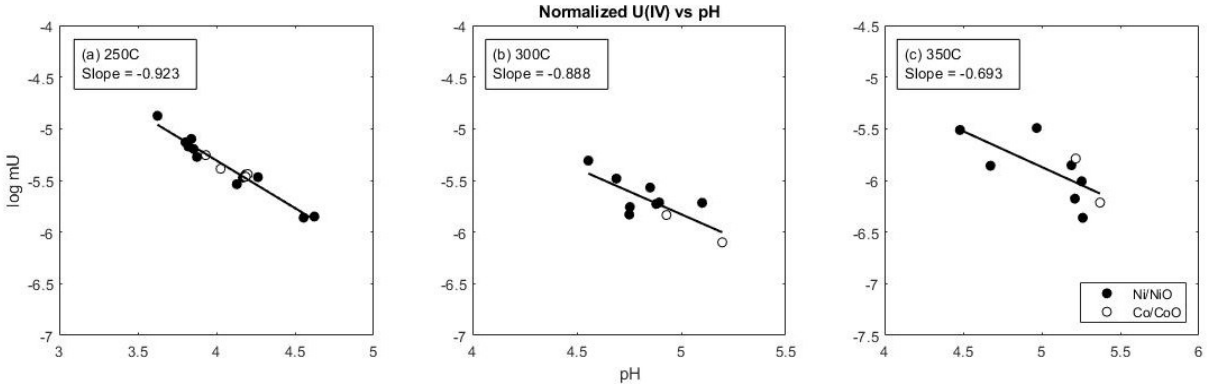

Figure 3.6 Normalized function of uranium concentrations versus pH

Logarithms of uranium molality normalized to log HSO_4^- activity of -2.5. Normalization is used to standardize experimental values to a fixed HSO_4^- activity so proper stoichiometric slopes can be observed when uranium concentrations is plotted against pH.

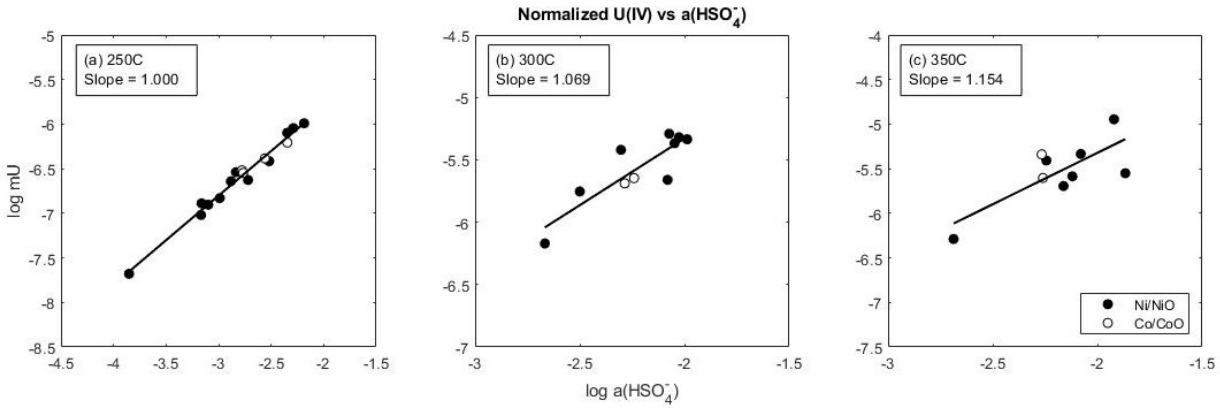

Figure 3.7 Normalized function of uranium concentrations vs HSO_4^- activity

Logarithms of uranium molality normalized to pH of 5. Normalization is used to standardize experimental values to a fixed pH so proper stoichiometric slopes can be observed when plotted against activity of HSO_4^-.

Data presented shows experiments with two redox buffers (Ni/NiO and Co/CoO). These are used to set the system's *f*O2 low enough to prevent U^{4+} from oxidizing to U^{6+}. The perfect agreement between data from both experiments (i.e. with Ni/NiO and Co/CoO) validates the assumption that the dissolution of UO_2 in all experiments is a redox-independent process and the species limiting uranium concentrations are U(IV) species (see figures 3.5-3.7). T Therefore, we conclude the solubility of UO_2 is controlled by the reaction:

$$O_2^{cryst} + HSO_4^- + H^+ = U(OH)_2SO_4^\circ \quad (3.1)$$

3.1.7 Data Reduction

To account for all system complexities, the OptimA (Hch software package) code is used to determine formation constants for each isotherm (Shvarov, 2010). The code minimizes the

sum of the squared deviations of measured, experimental concentrations of U from those theoretically calculated at equilibrium by adjusting the Gibbs free energy of the species of interest ($U(OH)_2SO_4$). To calculate the equilibrium state of the chemical system, the Hch package minimized its free energy.

At equilibrium, the system model also includes the following: Uraninite, Nickel, Bunsenite, U^{4+}, UOH^{2+}, UO^{+}, HUO_2, UO_2^{-}, UOH^{3+}, UO^{2+}, UO_2, HUO_2^{+}, HUO_3^{-}, UO_2^{+}, UO_2OH, UO_2^{2+}, UO_3^{-}, UO_2OH^{+}, UO_3, UO_4^{2-}, HUO_4^{-}, UO_2SO_4, $UO_2(SO_4)_2^{2-}$, UO_2Cl^{+}, UO_2Cl_2, UCl_4, plus all previously listed species used for pH_T calculations. Thermodynamic properties of these components are from Shock et al. (1997a), Shock et al. (1997b), Guillamont et al. (2003) , Timofeev et al. (2018), and Migdisov et al (2018). Thermodynamic properties of water and its dissociation constant are from the Haar-Gallagher-Kell mode (1984) and the Marshall and Franck (1981) model, respectively. Activity coefficients of charged species were calculated using the extended Debye-Huckel equation, and activity coefficients of neutral aqueous species were calculated from the simplified version of the extended Debye-Huckel equation:

$$\log \gamma_i = \Gamma + b_\gamma I \tag{3.2}$$

Using the thermodynamic data for Uraninite (Guillaumont et al., 2003), U^{4+} (Shock, Sassani, Willis, et al., 1997b), HSO_4^{-} and SO_4^{2-} (Johnson et al., 1992; Shock, Sassani, Willis, et al., 1997b), the optimized values of the Gibbs free energies were recalculated to the logarithms of the constants ($\log K = -\Delta rG/(2.303 \cdot RT)$) for the reaction in equation 3.1:

$$\Delta rG°_T = \Delta G°_T\,(U(OH)_2SO_4^{\circ}) - \Delta rG°_T\,(UO_2^{cryst}) - \Delta rG°_T\,(HSO_4^{-}) \tag{3.3}$$

Where

$$\Delta G°_T (H^+) = 0; \quad (3.4)$$

and for the formation reaction:

$$U^{4+} + SO_4^{2-} + 2OH^- = U(OH)_2SO_4 \quad (3.5)$$

$$\Delta rG°_T = \Delta G°_T (U(OH)_2SO_4^{\circ}) - \Delta rG°_T (U^{4+}) - \Delta rG°_T (SO_4^{2-}) - 2\,\Delta rG°_T (OH^-); \quad (3.6)$$

The derived formation constants, which provide ability to calculate the activity of a complex in a solution, are reported in Table 3.2, along with uncertainties calculated based on the confidence intervals returned by the OptimA code for $\Delta G°_T (U(OH)_2SO_4^{\circ})$. The trend of the obtained formation constant (log β) values as a function of temperature (-1000/T(K)) is also illustrated in figure 3.8.

Table 3.2 Formation constants for $U(OH)_2SO_4$

Reaction	Constant	250ºC	300ºC	350ºßC
$UO_2^{cryst} + HSO_4^- + H^+ = U(OH)_2SO_4^o$	log K	1.184 ± 0.11	1.647 ± 0.27	1.653 ± 0.32
$U^{4+} + SO_4^{2-} + 2OH^- = U(OH)_2SO_4$	log β	30.18	32.16	36.31

Logarithms of the formation constants for the species determined in this study.

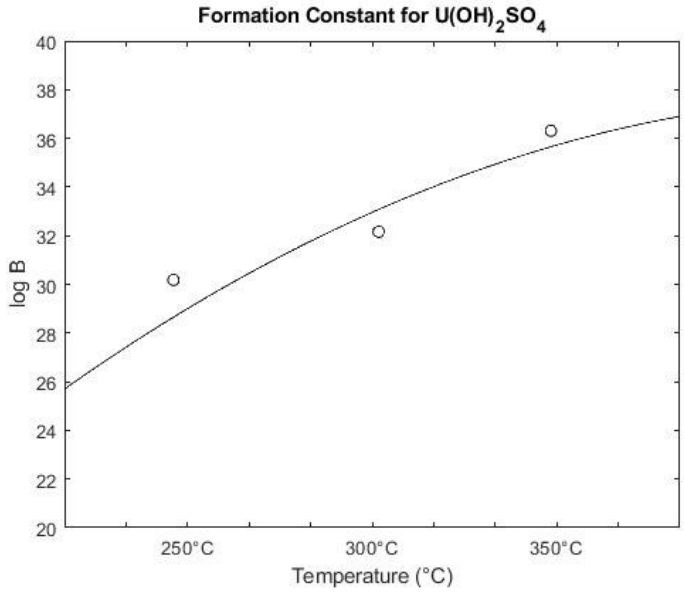

Figure 3.8 Formation constants for $U(OH)_2SO_4$

Logarithms of the formation constants for $U(OH)_2SO_4$ plotted as a function of temperature (-1000/T(K)).

In order to extrapolate these values to the temperatures beyond those investigated experimentally, the values of formation constants (log β) have been fitted to the Ryzhenko–Bryzgalin (MRB) mode (Ryzhenko, Bryzgalin, Artamkina, Spasennykh, & Shapkin, 1985) modified by Shvarov and Bastrakov (Y. V. Shvarov & Bastrakov, 1999). The latter is a model that was developed to fit the temperature and pressure dependence of dissociation constants for ion pairs in an aqueous solution:

$$logK_{(T,P)} = \frac{T_r}{T} logK_{(T_r,P_r)} + B_{(T,P)} * \left(Azz/_a + \frac{Bzz/_a}{T} \right) \quad (3.7)$$

where K is the dissociation constant of the ion pair, Tr, Pr are the reference temperature and pressure, and Azz/a and Bzz/a are fitting parameters. The term B(T,P) accounts for the properties

of water at temperature T and pressure and P, and is computed from the data of Marshall and Franck (1981). The parameters of this model for $U(OH)_2SO_4^\circ$ are reported in Table 3.3.

Table 3.3 Ryzhenko-Bryzgalin (MRB) parameters for $U(OH)_2SO_4$

	pK(298)	A (zz/a)	B (zz/b)
$U(OH)_2SO_4$	9.774	-4.876	6595.72

The Ryzhenko–Bryzgalin (MRB) model parameters for $U(OH)_2SO_4$ aqueous complex derived based on results of the experiments reported in this study.

3.2 General Discussion

Uranium concentrations experimentally determined at all isotherms are unexpectedly high compared to concentrations predicted using current thermodynamic data. In some experiments, they reach up to 3.5 ppm – at least seven orders of magnitude greater than concentrations predicted in a system without uranium sulfate or chloride complexes (based on the data reported in Shock et al. (1997a)).

Data from experiments illustrated in figure 3.8 show the stability of $U(OH)_2SO_4^\circ$ increases with temperature. That the species has low stability at ambient temperature explains why it has not been previously identified or included in the Guillamont et al. uranium dataset, which is mostly based on experimental data obtained at temperatures below 100°C. Guillamont et al. does account for sulfate complexation of U(IV), but suggests that ambient conditions are predominated by simple U(IV)-sulfate complexes, such as $U(SO_4)_2$ and USO_4^{2+} (Guillaumont et al., 2003). Identification of $U(OH)_2SO_4^\circ$ as the predominant sulfate species at elevated temperatures suggests changes in the speciation scheme and replaces simple sulfate complexation with mixed hydroxyl-sulfate complexes.

Although relatively uncommon, the formation of mixed ligand complexes involving hydroxyl complexes has been described for a few hard bases, such as Nb, Sn, Ta, Th, and Zr

(S.U. Aja, Wood, & Williams-Jones, 1995; Altmaier, Neck, Müller, & Fanghänel, 2005; Artaches A. Migdisov, Williams-Jones, van Hinsberg, & Salvi, 2011; Östhols, Bruno, & Grenthe, 1994; A. Timofeev, Migdisov, & Williams-Jones, 2015, 2017). For example, Zr speciation is temperature dependent in chloride-bearing solutions. At ambient temperature, simple fluoride complexes predominate (Aja, Wood, & Williams-Jones, 1995), but at elevated temperatures, hydroxyl-fluoride species predominate (Migdisov et al., 2011). Similar effects were found for Nb and Ta fluoride complexes (Timofeev, Migdisov, & Williams-Jones, 2015, 2017). In addition, hydroxyl-fluoride and hydroxyl-chloride complexes have been described for high-T speciation of Sn(IV) (Ryzhenko, Shvarov, & Kovalenko, 1997). It is notable that most of the species described in the above publications are neutrally charged, as is $U(OH)_2SO_4^\circ$. This is in a good agreement with the general trend for high-T speciation in aqueous solutions. An increase in temperature results in alteration of the positional and orientational constraints of water as a solvent, partial disruption of the 3D hydrogen bonding network which stabilizes highly charged species, and, thus, promotion of ion pairing/association and metal complex formation (Seward, Williams-Jones, & Migdisov, 2013).

Besides its neutrality, another characteristic feature of $U(OH)_2SO_4^\circ$ is its unexpectedly high stability at elevated temperatures. The traditional assumption on immobility of tetravalent uranium under reducing conditions (Allard, 1982; Carbol et al., 2005; Opel, Weiß, Hübener, Zänker, & Bernhard, 2007; Sani, Peyton, Amonette, & Geesey, 2004) was recently challenged by the study of Timofeev et al. (Timofeev et al., 2018), which demonstrated high mobility of uranium under reducing conditions and temperature above 200ºC. The additional criterium, necessary for uranium immobilization, is the availability of appropriate ligands (Cl in the case of Timofeev et al. (Timofeev et al., 2018) study) for complexation with U(IV). The experiments of

Timofeev et al. (Timofeev et al., 2018) were performed at appreciably acidic conditions (pH_T<2.5-3.0) and showed that the ability of chloride-bearing fluid to carry uranium decreases by four orders of magnitude when pH increases by one unit. As conditions move toward weakly acidic and near neutral, this ability of chloride solutions to transport U(IV) become insignificant. Results show that at pH higher than 2, sulfate can become a key player in mobilization and transport of U(IV).

3.2.1 Uranium Mobility at Low and Intermediate pH

Figure 3.9 illustrates the effects of increasing sulfate on total dissolved uranium in systems at 300ºC and low (2) and intermediate (5) pH. It is clear that the uranium-chloride complexes contribute minimally at low pH conditions, but not at intermediate pH conditions. This in contrast the $U(OH)_2SO_4^\circ$ species identified in this study, which remain significant at near-neutral conditions. Chloride species play a significant role in only the low pH system, but the $U(OH)_2SO_4^\circ$ species is still able to concentrate uranium up to several parts per million at an intermediate pH.

The species distribution diagrams in Figure 3.9 were calculated for a system saturated with respect to UO_2 at a temperature of 300°C. To illustrate the competition between chloride and sulfate complexes, the system includes 1m NaCl, while varying sulfate over the range of 10^{-2} to 10^{-7} m Na_2SO_4. The results are consistent with the findings of Timofeev at al.: at highly acidic, low sulfate concentration solutions, chloride complexes are highly influential in uranium transport. However, increases in either pH (approaching 5) or sulfate (approaching 10^{-5} m Na_2SO_4) lead to dramatic reduction of chloride importance and increased transport ability through this study's sulfate complex.

Figure 3.9b represents the more realistic scenario of the two, since highly acidic conditions are not often common in natural conditions expected at nuclear waste repository sites. Nevertheless, it is notable, for both scenarios, that the reduced uranium species limit total uranium solubility, since oxidized (U^{6+}) species are not appreciable at concentrations presented (see fig. 3.9). Consequently, the findings presented here suggest that re-evaluation may be necessary for models of high temperature, uranium-bearing, ore-forming systems.

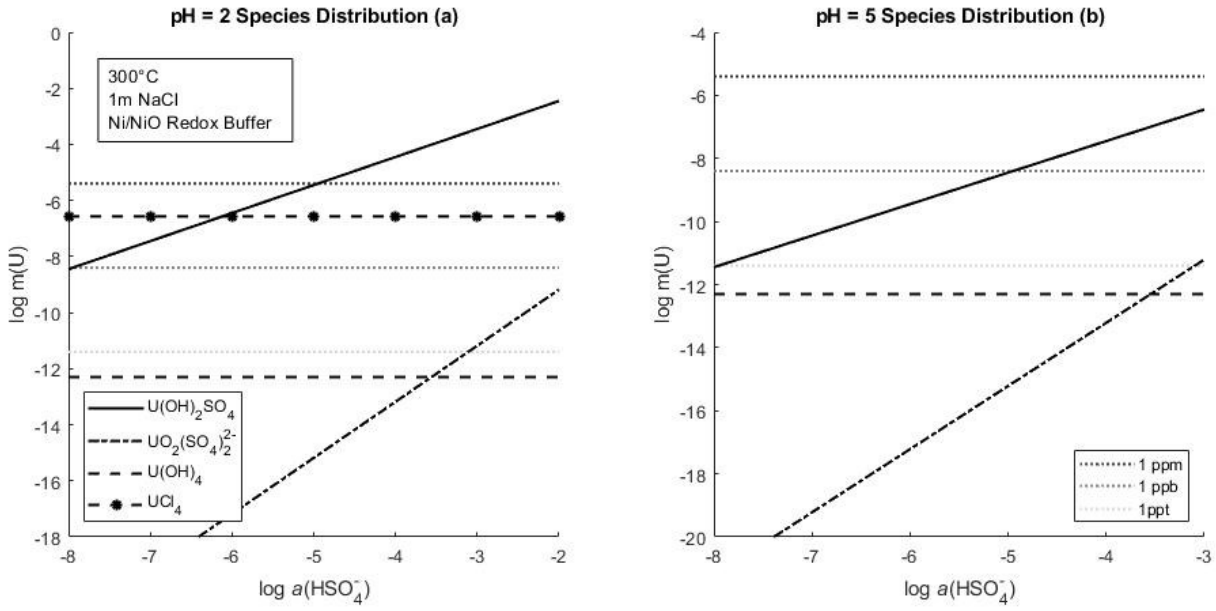

Figure 3.9 $U(OH)_2SO_4^{\circ}$ transport ability at low and intermediate pH_T

Distribution of predominant species at pH of 2 (a) and 5 (b) at 300ºC and conditions corresponding to Ni/NiO buffers. Logarithms of uranium molality of each species are plotted against logarithms of sulfate activity over the range of 10^{-2} – 10^{-7} m Na_2SO_4. Log m U axis bars indicate 1 ppt, ppm, and ppb of U.

3.2.2 Ore-forming System Application

While the primary application of this work is linked to waste disposal problem, the sulfate species is also important to ore-forming systems as well. These systems are highly variable in pH conditions. While some ore systems can be described using the uranium chloride complexes, others are characterized by more neutral pH conditions. Ore-forming systems such as Cigar Lake, Canada, Jachymov, Czech Republic, and the Oklo natural reactor in Gabon, Africa are all reducing systems analogous to the proposed granitic disposal sites (Brookins, 1990; Casas et al., 1998; Sunder et al., 1996). The results of this work also demonstrate the contribution of sulfate in facilitating uranium transport, observable in the neutral pH range species distributions.

CHAPTER IV

WASTE DISPOSAL SITE SCENARIOS

4.1 Waste Disposal Introduction

Effective nuclear waste disposal is contingent upon many factors, but its primary objective is preventing actinide (and other radionuclides) exposure to water. Once UO_2, the principle component of spent nuclear fuel (Burns, Ewing, & Navrotsky, 2012), is exposed to water, transport can be facilitated through a variety of mechanisms, including changes in redox states, speciation with available ligands, and hydrothermal mobilization of uranium. To assess the safety of a proposed nuclear waste repository, it is necessary to quantify these effects to the greatest degree possible. The work in this study provides improved ability to model uranium transport in waste disposal sites, since the groundwater at some proposed locations is abundant in sulfur. The following sections will describe the system of interest, importance of uranium sulfate complexes, and detail the scope of the nuclear waste disposal problem in new light of this study's findings.

4.2 Input Parameter Selection

The findings for the sulfate experiments are particularly important due to their implications for uranium mobilization in hydrothermal systems, such as the waste repository setting. Groundwater and chemical conditions at proposed waste disposal sites are similar to experimental conditions in this study, and thus can be used as parameters for uranium transport simulations using the new data for $U(OH)_2SO_4^\circ$. Conditions for scenarios presented in this study

come from waters documented at the Waste Isolation Pilot (WIPP), as this is the only active repository in the United States, and the Grimsel Test Site, a geological disposal test site in Switzerland (Felmy et al., 1997; Missana & Geckeis, 2006). Sulfate concentrations at these two locations ranges from 0.18 to 0.35 mol/kg ; in addition, experimental studies have suggested these concentrations could increase more if sulfide minerals decompose in common bentonite backfill (Caporuscio et al., 2017; M. C. Cheshire et al., 2018; Michael C. Cheshire et al., 2014).

4.3 Species Distribution Results

Scenarios illustrating the ability of sulfate to transport uranium in a repository setting are provided by using the HcH software package to calculate species distributions. After inputting the newly derived thermodynamic constants for the $U(OH)_2SO_4$ species, the software simulates the composition of a fluid given inputs of temperature, pressure, and ligand concentrations. As can be seen from figure 4.1, even at significantly lower sulfate concentrations than employed in this study, it is still the $U(OH)_2SO_4$ species which limits uranium solubility, and can elevate mobile, aqueous uranium to levels approaching 1 ppm. Temperature has a strong effect on these distributions. As it drops below 200°C, the total dissolved uranium is predicted to decrease to less than 1 ppt (parts per trillion) for systems with sulfate concentrations equal to concentrations likely to be found in repository groundwaters. The contrast between low and high temperature speciation necessitates using update thermodynamic databases, complete with high temperature species.

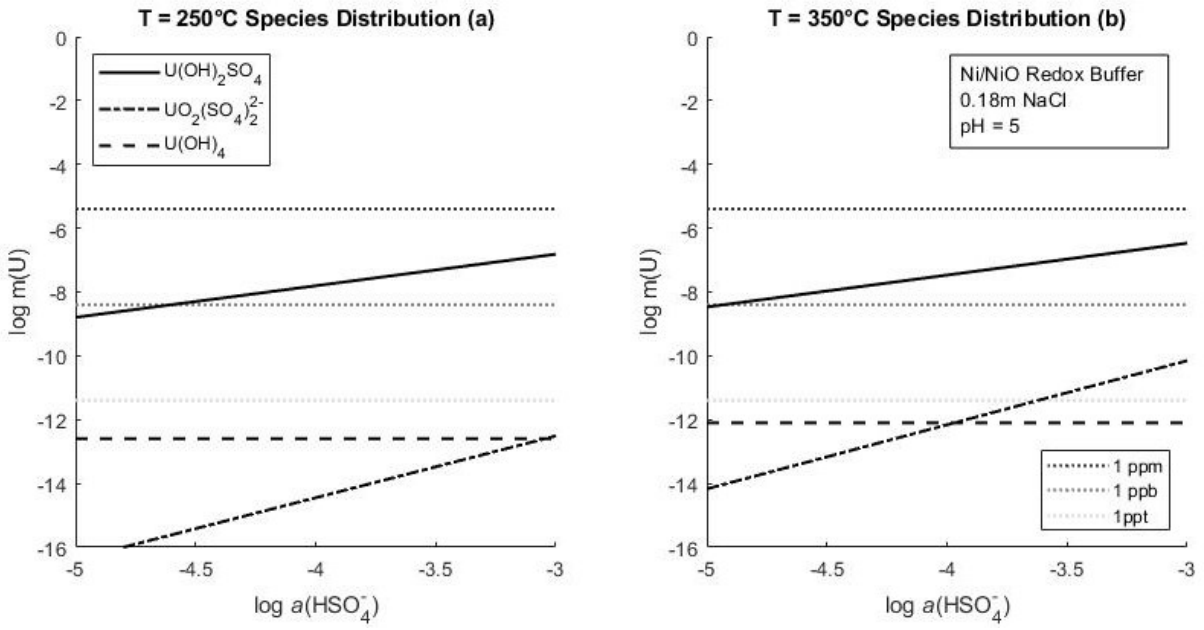

Figure 4.1 $U(OH)_2SO_4^\circ$ transport ability at waste disposal site conditions

Distribution of predominant species at a pH of 5 at (a) 250, (b) 350 ºC – conditions similar to nuclear waste disposal sites. Concentrations are calculated for solutions saturated with respect to solid UO_2, and logarithms of uranium molality of each species are plotted against logarithms of total sulfate over the range of 50 – 300 ppm Na_2SO_4.

4.4 Model Scenarios

In contrast to models that do not include U(IV) species, the repository setting presented here shows that reduced species do, indeed, have notable importance. These species must be a consideration when determining a repository site. Proper modelling will lead to a more reliable long term, underground storage option. As can be seen in figure 4.1, reduced species unequivocally have potential for mobilizing uranium in even reduced repository conditions.

Nuclear plants typically generate over 20 tons of waste annually, which leads the question of where to store this waste. According to the current protocol, the nuclear waste is stored above ground level, which is only a temporary solution. Long term, underground storage

seeks to minimize the spread of contamination during a potential catastrophic event, such as a waste canister containment breach. In this scenario, the spent nuclear fuel is exposed to groundwater, and reliable models will provide estimates for transport. A containment breach in the first 200 years of a spent nuclear fuel canister would result in interaction with water at elevated temperature as result of radionuclide decay occurring in nuclear waste(Hardin et al., 2013). The scenario in Figure 4.1 demonstrates that sulfate concentrations commonly occurring in groundwater are able to mobilize uranium to ppb level concentrations and thus facilitate its transport at or above 250ºC. By omitting U(IV) species from repository models, the mobility to uranium in the solution is significantly underestimated.

The results of this study on uranium behavior at reducing conditions and elevated temperatures suggest that aqueous transport of uranium could be a significant, catastrophic event. Therefore, a special attention is required in developing or improving engineered barrier systems for immobilizing dissolved uranium.

4.5 Final Remarks

The solubility of UO_2 in high temperature, aqueous, reduced systems was investigated. Data presented in this study suggest unexpectedly high stability of the predominant, neutrally charged, aqueous $U(OH)_2SO_4^\circ$ species above 250°C. This work builds upon existing findings of high temperature speciation, and contrast with the standard paradigm that reduced conditions ensure immobility. In contrast to the U(IV) chloride complexes, the new sulfate species is much more stable in intermediate pH systems, and can increase total uranium mobility even as pH approaches near-neutral conditions.

The findings were applied to simulate transport at natural low to intermediate pH groundwater environments, as well as expected conditions at proposed nuclear waste repository

and disposal testing sites. The role of sulfate is emphasized: within realistic ranges of sulfate compositions, aqueous uranium concentrations can exceed ppm level when in equilibrium with Uraninite (UO_2). These implications are crucial for establishing improved safety protocol and will aid in the modelling of ore forming processes and repository setting.

REFERENCES

Ahonen, L., Ervanne, H., Jaakkola, T., & Blomqvist, R. (1994). Redox chemistry in uranium-rich groundwater of Palmottu uranium deposit, Finland. *Radiochimica Acta*, *66/67*, 115–121.

Aja, S. U., Wood, S. A., & Williams-jones, A. E. (1995). The aqueous geochemistry of Zr and the solubility of some Zr-bearing minerals. *Applied Geochemistry*, *10*(6), 603–620.

Aja, S. U., Wood, S. A., & Williams-Jones, A. E. (1995). The aqueous geochemistry of Zr and the solubility of some Zr-bearing minerals. *Applied Geochemistry*, *10*(6), 603–620. https://doi.org/10.1016/0883-2927(95)00026-7

Allard. (1982). Solubilities of Actinides in Neutral or Basic Solutions. *Actinides in Perspective*, (Iii), 553–580. https://doi.org/10.1016/B978-0-08-029193-2.50029-8

Altmaier, M., Neck, V., Müller, R., & Fanghänel, T. (2005). Solubility of ThO2·xH2O(am) in carbonate solution and the formation of ternary Th(IV) hydroxide-carbonate complexes. *Radiochimica Acta*, *93*(2), 83–92. https://doi.org/10.1524/ract.93.2.83.59420

Anderson, G. M., & Crerar, D. A. (1993). *Thermodynamics in geochemistry: The equilibrium model*. Oxford University Press on Demand.

Bastrakov, E. N., Jaireth, S., & Mernagh, T. P. (2010). Solubility of uranium in hydrothermal fluids at 25° to 300°C Implications for the formation of uranium deposits. In *Geoscience Australia, Record 2010/29*.

Brookins, D. G. (1990). Radionuclide behabior at the Oklo nuclear reactor, gabon. *Waste Management*, *10*(X), 285–296.

Burns, P. C., Ewing, R. C., & Navrotsky, A. (2012). Nuclear fuel in a reactor accident. *Science*, *335*(6073), 1184–1188. https://doi.org/10.1126/science.1211285

Caporuscio, F. A., Palaich, S. E. M., Cheshire, M. C., & Jové Colón, C. F. (2017). Corrosion of copper and authigenic sulfide mineral growth in hydrothermal bentonite experiments. *Journal of Nuclear Materials*, *485*, 137–146. https://doi.org/10.1016/j.jnucmat.2016.12.036

Carbol, P., Cobos-Sabate, J., Glatz, J.-P., Ronchi, C. ., Rondinella, V., Loida, a., … Martínez-Esparza, a. (2005). *TR-05-09 on the dissolution of 233 U doped*. *2*(March 2005), 139.

Casas, I., De Pablo, J., Giménez, J., Torrero, M. E., Bruno, J., Cera, E., … Ewing, R. C. (1998). The role of pe, pH, and carbonate on the solubility of UO2 and uraninite under nominally reducing conditions. *Geochimica et Cosmochimica Acta*, *62*(13), 2223–2231. https://doi.org/10.1016/S0016-7037(98)00140-9

Cheshire, M. C., Caporuscio, F. A., Jové Colón, C. F., & Norskog, K. E. (2018). Fe-saponite growth on low-carbon and stainless steel in hydrothermal-bentonite experiments. *Journal of Nuclear Materials*, *511*, 353–366. https://doi.org/10.1016/j.jnucmat.2018.09.038

Cheshire, M. C., Caporuscio, F. A., Rearick, M. S., Jové-Colón, C., & McCarney, M. K. (2014). Bentonite evolution at elevated pressures and temperatures: An experimental study for generic nuclear repository designs. *American Mineralogist*, *99*(8–9), 1662–1675. https://doi.org/10.2138/am.2014.4673

Cuney, M. (2009). The extreme diversity of uranium deposits. *Mineral. Deposita*, *44*, 3–9.

Ellis, G. S., Sessions, A. L., Deev, A., Aizenshtat, Z., Adkins, J. F., Tang, Y., … Amrani, A. (2016). Study of thermochemical sulfate reduction mechanism using compound specific sulfur isotope analysis. *Geochimica et Cosmochimica Acta*, *188*, 73–92. https://doi.org/10.1016/j.gca.2016.05.026

Felmy, A. R., ONISHI, L. M., FOSTER, N. S., RUSTAD, J. R., RAI, D., & MASON, M. J. (1997). An aqueous thermodynamic model for the Pb2+–Na+–K+–Ca2+–Mg2+–H+–Cl-–SO4 2-– H2O system to high concentration: Application to WIPP brines. *Geochimica et Cosmochimica Acta*, *64*(21), 3615–3628.

Gammons, C. H., Wood, S. A., Jonas, J. P., & Madison, J. P. (2003). Geochemistry of the rare-earth elements and uranium in the acidic Berkeley Pit lake, Butte, Montana. *Chemical Geology*, *198*(3–4), 269–288. https://doi.org/10.1016/S0009-2541(03)00034-2

Goldstein, T. P., & Aizenshtat, Z. (1994). Thermochemical sulfate reduction a review. *Journal of Thermal Analysis*, *42*(1), 241–290. https://doi.org/10.1007/BF02547004

Grenthe, I., J., F., Konings, R. J. M., R.J., L., A.B., M., C., N.-T., … Forest, I. (1992). Chemical Thermodynamics of Uranium. In *Nuclear Energy Agency*.

Guillaumont, R. (Robert), Fanghanel, T., Neck, V., Fuger, J., Palmer, D. A., Grenthe, I., … OECD Nuclear Energy Agency. (2003). Update on the chemical thermodynamics of uranium, neptunium, plutonium, americium and technetium. *Chemical Thermodynamics*, *5*, 919. Retrieved from https://books.google.de/books/about/Update_on_the_Chemical_Thermodynamics_of.html?id=J9zvAAAAMAAJ&redir_esc=y

Guillaumont, R., Fanghanel, T., Neck, V., Fuger, J., Palmer, D. A., Grenthe, I., & Rand, M. H. (2003). Update on the chemical thermodynamics of uranium, neptunium, plutonium, americium and technetium. *Chemical Thermodynamics*, *5*, 919. Retrieved from https://books.google.de/books/about/Update_on_the_Chemical_Thermodynamics_of.html?id=J9zvAAAAMAAJ&redir_esc=y

Hardin, E. L., Clayton, D. J., Howard, R. L., Scaglione, J. M., Pierce, E., Banerjee, K., … Nutt, W. M. (2013). Preliminary Report on Dual-Purpose Canister Disposal Alternatives (FY13). In *FCRD-UFD-2013-000171 Rev. 1, prepared for the US Department of Energy, Office of Used Nuclear Fuel Disposition*.

Haynes, D., Cross, K., Bills, R., & Reed, M. (1995). Haynes1995 Olympic Dam Ore Genesis.pdf. *Economic Geology*, *90*, 281–307.

Helgeson, H. C., Kirkham, D. H., & Flowers, G. C. (1981). Theoretical prediction of the thermodynamic behavior of aqueous electrolytes at high pressures and temperatures: IV. Calculation of activity coefficients, osmotic coefficients, and apparent molal and standard and relative partial molal properties to 600 °. *Am. J. Sci.*, *281*, 1249–1516.

Hennig, C., Schmeide, K., Brendler, V., Moll, H., Tsushima, S., & Scheinost, A. C. (2007). EXAFS investigation of U(VI), U(IV), and Th(IV) sulfato complexes in aqueous solution. *Inorganic Chemistry*, *46*(15), 5882–5892. https://doi.org/10.1021/ic0619759

Johnson, J. W., Oelkers, E. H., & Helgeson, H. C. (1992). SUPCRT92: A software package for calculating the standard molal thermodynamic properties of minerals, gases, aqueous species, and reactions from 1 to 5000 bar and 0 to 1000 °C. *Computers & Geosciences*, *18*(7), 899–947. https://doi.org/10.1016/0098-3004(92)90029-Q

Kestin, J., Sengers, J., & Kamgar-Parsi, B. (1984). Thermophysical Properties of Fluid H20. *J. Phys. Chem. Ref.*, *13*(1), 175–183. Retrieved from http://potomac.nist.gov/srd/PDFfiles/jpcrd250.pdf

Kister, P., Vieillard, P., Cuney, M., Quirt, D., & Laverret, E. (2005). Thermodynamic constraints on the mineralogical and fluid composition evolution in a clastic sedimentary basin: the Athabasca Basin (Saskatchewan, Canada). *European Journal of Mineralogy*, *17*(2), 325–341. https://doi.org/10.1127/0935-1221/2005/0017-0325

Komninou, A., & Sverjensky, D. A. (1995). Hydrothermal alteration and the chemistry of ore-forming fluids in an unconformity-type uranium deposit. *Geochimica et Cosmochimica Acta*, *59*(13), 2709–2723. https://doi.org/10.1016/0016-7037(95)00167-X

Li, H., Cai, C., Jia, L., Xu, C., & Zhang, K. (2017). The Effect of Water Chemistry on Thermochemical Sulfate Reduction: A Case Study from the Ordovician in the Tazhong Area, Northwest China. *Geofluids*, *2017*. https://doi.org/10.1155/2017/6351382

Marshall, W., & Franck, E. U. (1981). Ion product of water substance, 0-1000 °C, 1-10,000 bars. *Journal of Physical & Chemical Reference Data*, *10*, 295–304.

Migdisov, A. A., Boukhalfa, H., Timofeev, A., Runde, W., Roback, R., & Williams-Jones, A. E. (2018). A spectroscopic study of uranyl speciation in chloride-bearing solutions at temperatures up to 250 °C. *Geochimica et Cosmochimica Acta*, *222*, 130–145. https://doi.org/10.1016/j.gca.2017.10.016

Migdisov, A. A., Williams-Jones, A. E., van Hinsberg, V., & Salvi, S. (2011). An experimental study of the solubility of baddeleyite (ZrO2) in fluoride-bearing solutions at elevated temperature. *Geochimica et Cosmochimica Acta*, *75*(23), 7426–7434.

Millero, F. J., Feistel, R., Wright, D. G., & McDougall, T. J. (2008). The composition of Standard Seawater and the definition of the Reference-Composition Salinity Scale. *Deep-Sea Research Part I: Oceanographic Research Papers*, *55*(1), 50–72. https://doi.org/10.1016/j.dsr.2007.10.001

Missana, T., & Geckeis, H. (2006). *Grimsel Test Site–Investigation Phase V. The CRR Final Project Report Series II: Supporting Laboratory Experiments with Radionuclides and Bentonite Colloids*.

Oelkers, E., & Helgeson, H. C. (1990). Triple-ion anions and polynuclear complexing in supercritical electrolyte solutions. *Geochimica et Cosmochimica Acta*, *54*(3), 727–738. https://doi.org/10.1016/0016-7037(90)90368-U

Oelkers, E., & Helgeson, H. C. (1991). Calculation of activity coefficients and degrees of formation of neutral ion pairs in supercritical electrolyte solutions. *Geochimica et Cosmochimica Acta*, *55*(5), 1235–1251. https://doi.org/10.1016/0016-7037(91)90303-M

Opel, K., Weiß, S., Hübener, S., Zänker, H., & Bernhard, G. (2007). Study of the solubility of amorphous and crystalline uranium dioxide by combined spectroscopic methods. *Radiochimica Acta*, *95*(3), 143–149. https://doi.org/10.1524/ract.2007.95.3.143

Östhols, E., Bruno, J., & Grenthe, I. (1994). On the influence of carbonate on mineral dissolution: III. The solubility of microcrystalline ThO2 in CO2-H2O media. *Geochimica et Cosmochimica Acta*, *58*(2), 613–623. https://doi.org/10.1016/0016-7037(94)90492-8

Parks, G. A., & Pohl, D. C. (1988). Hydrothermal solubility of uraninite. *Geochimica et Cosmochimica Acta*, *52*(4), 863–875. https://doi.org/10.1016/0016-7037(88)90357-2

Perez, F. M., Gil, J. M., & Gil, F. J. M. (1980). *Preparation, Infrared and Visible Spectra of Sulfate Complexes of Uraniumm(IV)*. *240*, 231–240.

Rich, R. A., Holland, H. D., & Peterson, U. (1977). *Hydrothermal Uranium Deposits*.

Richard, A., Rozsypal, C., Mercadier, J., Banks, D. a., Cuney, M., Boiron, M.-C., & Cathelineau, M. (2011). Giant uranium deposits formed from exceptionally uranium-rich acidic brines. *Nature Geoscience*, *5*(2), 142–146. https://doi.org/10.1038/ngeo1338

Ryzhenko, B. N., Bryzgalin, O. V., Artamkina, I. Y., Spasennykh, M. Y., & Shapkin, A. I. (1985). An electrostatic model for the electrolytic dissociation of inorganic substances dissolved in water. *Geochem. Int.*, *22*, 138–144.

Ryzhenko, B. N., Shvarov, Y. V., & Kovalenko, N. I. (1997). The Sn-Cl-FCSHO-Na system: Thermodynamic properties of components within the conditions of the earth's crust. *Geochemistry International*, *35*, 1016–1020.

Sani, R. K., Peyton, B. M., Amonette, J. E., & Geesey, G. G. (2004). Reduction of uranium(VI) under sulfate-reducing conditions in the presence of Fe(III)-(hydr)oxides. *Geochimica et Cosmochimica Acta*, *68*(12), 2639–2648. https://doi.org/10.1016/j.gca.2004.01.005

Seward, T. M., Williams-Jones, A. E., & Migdisov, A. A. (2013). The Chemistry of Metal Transport and Deposition by Ore-Forming Hydrothermal Fluids. In *Treatise on Geochemistry: Second Edition* (2nd ed., Vol. 13). https://doi.org/10.1016/B978-0-08-095975-7.01102-5

Shock, E. L., Sassani, D. C., & Betz, H. (1997). Uranium in geologic fluids: Estimates of standard partial molal properties, oxidation potentials, and hydrolysis constants at high temperatures and pressures. *Geochimica et Cosmochimica Acta*, *61*(20), 4245–4266. https://doi.org/10.1016/S0016-7037(97)00240-8

Shock, E. L., Sassani, D. C., Willis, M., & Sverjensky, D. A. (1997a). Inorganic species in geologic fluids: correlations among standard molal thermodynamic properties of aqueous ions and hydroxide complexes. *Geochimica et Cosmochimica Acta*, *61*(5), 907–950.

Shock, E. L., Sassani, D. C., Willis, M., & Sverjensky, D. A. (1997b). Inorganic species in geologic fluids: Correlations among standard molal thermodynamic properties of aqueous ions and hydroxide complexes. *Geochimica et Cosmochimica Acta*, *61*(5), 907–950. https://doi.org/10.1016/S0016-7037(96)00339-0

Shvarov, Y. V., & Bastrakov, E. N. (1999). *HCh, A Software Package for Geochemical Equlibrium Modeling: User's Guide. Record 1999/25*.

Shvarov, Y. V. (2010). OptimA: A program for the calculation of the free energies of dissolved aqueous species from the results of chemical experiments.

Sunder, B. S., Cramer, J. J., & Miller, N. H. (1996). *Geochemistry of the Cigar Lake Uranium Deposit : XPS Studies*. *307*, 303–307.

Sverjensky, D., Shock, E. L., & Helgeson, H. C. (1997). Prediction of the thermodynamic properties of aqueous metal complexes to 1000 °C and 5kb. *Geochimica et Cosmochimica Acta*, *61*, 1359–1412.

Tagirov, B. R., Zotov, A., & Akinfiev, N. (1997). Experimental study of dissociation of HCl from 350 to 500° C and from 500 to 2500 bars: Thermodynamic properties of HCl°(aq). *Geochimica et Cosmochimica Acta*, *61*(20), 4267–4280. https://doi.org/10.1016/S0016-7037(97)00274-3

Thom, J., & Anderson, G. M. (2008). The role of thermochemical sulfate reduction in the origin of Mississippi Valley-type deposits. I. Experimental results. *Geofluids*, *8*(1), 16–26. https://doi.org/10.1111/j.1468-8123.2007.00201.x

Timofeev, A., Migdisov, A. A., & Williams-Jones, A. E. (2015). An experimental study of the solubility and speciation of niobium in fluoride-bearing aqueous solutions at elevated temperature. *Geochimica et Cosmochimica Acta*, *158*, 103–111. https://doi.org/10.1016/j.gca.2011.09.043

Timofeev, A., Migdisov, A. A., & Williams-Jones, A. E. (2015). An experimental study of the solubility and speciation of niobium in fluoride-bearing aqueous solutions at elevated temperature. *Geochimica et Cosmochimica Acta*, *158*, 103–111.

Timofeev, A., Migdisov, A. A., & Williams-Jones, A. E. (2017). An experimental study of the solubility and speciation of tantalum in fluoride-bearing aqueous solutions at elevated temperature. *Geochimica et Cosmochimica Acta*, *197*, 294–304.

Timofeev, A., Migdisov, A. A., & Williams-Jones, A. E. (2017). An experimental study of the solubility and speciation of tantalum in fluoride-bearing aqueous solutions at elevated temperature. *Geochimica et Cosmochimica Acta*, *197*, 294–304.

Timofeev, A., Migdisov, A. A., Williams-Jones, A. E., Roback, R., Nelson, A. T., & Xu, H. (2018). Uranium transport in acidic brines under reducing conditions. *Nature Communications*, *9*(1), 1–7. https://doi.org/10.1038/s41467-018-03564-7

Tremaine, P., Chen, J., Wallace, G. I., & Boivin, W. A. (1981). Solubility of uranium (IV) oxide in alkaline aqueous solutions to 300 C. *Journal of Solution Chemistry*, *10*(3), 221–230. Retrieved from http://link.springer.com/article/10.1007/BF00653099